A Surface Reconstruction Route to High Productivity and Selectivity in CO_2 Electroreduction toward C_{2+} Hydrocarbons

*Md Golam Kibria, Cao-Thang Dinh, Ali Seifitokaldani, Phil De Luna, Thomas Burdyny, Rafael Quintero-Bermudez, Michael B. Ross, Oleksandr S. Bushuyev, F. Pelayo García de Arquer, Peidong Yang, David Sinton, and Edward H. Sargent**

Electrochemical carbon dioxide reduction (CO_2) is a promising technology to use renewable electricity to convert CO_2 into valuable carbon-based products. For commercial-scale applications, however, the productivity and selectivity toward multi-carbon products must be enhanced. A facile surface reconstruction approach that enables tuning of CO_2-reduction selectivity toward C_{2+} products on a copper-chloride (CuCl)-derived catalyst is reported here. Using a novel wet-oxidation process, both the oxidation state and morphology of Cu surface are controlled, providing uniformity of the electrode morphology and abundant surface active sites. The Cu surface is partially oxidized to form an initial Cu (I) chloride layer which is subsequently converted to a Cu (I) oxide surface. High C_{2+} selectivity on these catalysts are demonstrated in an H-cell configuration, in which 73% Faradaic efficiency (FE) for C_{2+} products is reached with 56% FE for ethylene (C_2H_4) and overall current density of 17 mA cm^{-2}. Thereafter, the method into a flow-cell configuration is translated, which allows operation in a highly alkaline medium for complete suppression of CH_4 production. A record C_{2+} FE of ≈84% and a half-cell power conversion efficiency of 50% at a partial current density of 336 mA cm^{-2} using the reconstructed Cu catalyst are reported.

The need to store intermittent renewable energy motivates the electroproduction of fuels and feedstocks. One such process, the electrochemical CO_2 reduction reaction (CO_2-RR), enables the conversion of CO_2 into valuable hydrocarbons and alcohols.[1–3] However, to become competitive with traditional fossil fuel-based technologies, the conversion efficiency and product selectivity for multicarbon products using the electrochemical approaches need to be improved from current levels.[4–6]

Today, copper-based catalysts are the most promising materials for selective reduction of CO_2 to multicarbon hydrocarbons.[7,8] High selectivity toward C_{2+} products, including ethylene (C_2H_4), ethanol (C_2H_5OH), and propanol (C_3H_7OH), has been demonstrated using Cu-based catalyst materials.[9–12]

Mechanisms underlying the improved selectivity often involve the initial material oxidation state.[8,13,14] For example, residual subsurface oxygen,[15] grain boundaries,[16] and unconverted Cu^+ states[17,18] have been reported to enhance CO adsorption and reduce the energy barrier for CO–CO coupling. Overall, research points to the final active surface species being a function of the Cu(I) or Cu(II) present on the surface prior to and after the CO_2 reduction reaction.[19] The sensitivity of the observed catalytic performance to

Prof. Md G. Kibria,[+] Dr. C.-T. Dinh, Dr. A. Seifitokaldani, R. Quintero-Bermudez, Dr. O. S. Bushuyev, Dr. F. P. García de Arquer, Prof. E. H. Sargent
Department of Electrical and Computer Engineering
University of Toronto
10 King's College Road, Toronto, ON M5S 3G4, Canada
E-mail: ted.sargent@utoronto.ca

P. De Luna
Department of Materials Science and Engineering
University of Toronto
Toronto, ON, Canada 184 College St, Toronto, ON M5S 3E4, Canada

The ORCID identification number(s) for the author(s) of this article can be found under https://doi.org/10.1002/adma.201804867.

[+]Present address: Department of Chemical and Petroleum Engineering, University of Calgary, 2500 University Drive, NW Calgary, Alberta T2N 1N4, Canada

[++]Present address: Materials for Energy Conversion and Storage, Department of Chemical Engineering, Delft University of Technology, 2629 HZ Delft, The Netherlands

Dr. T. Burdyny,[++] Prof. D. Sinton
Department of Mechanical and Industrial Engineering
University of Toronto
5 King's College Road, Toronto, ON M5S 3G8, Canada

Dr. M. B. Ross, Prof. P. Yang
Bio-inspired Solar Energy Program
Canadian Institute for Advanced Research
Toronto, Ontario M5G 1Z8, Canada

Dr. M. B. Ross, Prof. P. Yang
Department of Chemistry
University of California
Berkeley, Berkeley, CA 94720, USA

Prof. P. Yang
Department of Materials Science and Engineering
University of California
Berkeley, Berkeley, CA 94720, USA

Prof. P. Yang
Materials Sciences Division
Lawrence Berkeley National Laboratory
Berkeley, CA 94720, USA

DOI: 10.1002/adma.201804867

subtle changes in the initial and final condition highlights the need for the generation of consistent active sites across the surface of the catalyst.

Experimental[20] and modeling[21] efforts have also highlighted the importance of catalyst surface morphology on C_{2+} selectivity in CO_2-RR. This can suppress the primary competing reaction products including H_2 and CH_4. In general, it has been reported that high electrode pH conditions are required to enhance C_{2+} product selectivity by lowering the C—C coupling energy barrier, and shifting CH_4 formation to higher potentials.[18,22]

Since dissolved CO_2 exists only in neutral and low pH electrolytes, the local pH at the electrode must be raised by increasing the reaction current density in conjunction with using a low buffering bulk electrolyte, typically 0.1 M $KHCO_3$. While this suppresses CH_4 formation to less than 5% in some cases, the amount of CO_2 able to reach the catalyst's surface is also reduced. High C_2H_4 selectivity of up to 60% can then be achieved at the cost of low overall current densities (20 mA cm^{-2}),[18] highlighting a limitation in the current application of the catalyst. Other factors such as electrochemically active surface area and morphology-induced mass transport must further be taken into consideration as these can impact local reaction conditions across the surface of the catalyst, and subsequently the final selectivity toward multicarbon products.[23]

Previous oxide-derived Cu catalysts have been created by a number of different processes including O_2 plasma treatment,[18] electrodeposition of cuprous oxide (Cu_2O),[24] reduction of copper salts,[17] metal-ion cycling,[25] and thermal treatment of metallic Cu in air.[26] Despite the same underlying reaction mechanisms suspected to be at play in each case, wide ranges of C_{2+} product selectivities and current densities have been observed experimentally. These variations may arise from different proportions of the initial oxidation states on the catalyst's surface (Cu(0), Cu(I), Cu(II)), the distribution of these oxidation states across the catalyst surface, and the thickness of the formed oxide layer itself. Each of these factors independently affects the electrochemical reduction of the oxide layer into the final catalytic state as well as the final distribution and number of active sites. These examples combined present a need for both a simple procedure to oxidize a bare copper electrocatalyst, and ensure the presence of abundant active surface sites and the associated surface morphology that favors high selectivity toward C_{2+} products.

Here, we report a surface reconstruction approach that enables us to tune the hydrocarbon selectivity of a CuCl-derived catalyst. Using a wet-oxidation process, we are able to control both the oxidation state and morphology of a Cu surface, providing uniformity of the electrode morphology and the number of the surface active sites on the catalyst. The controlled growth of an initial CuCl layer provides a Cu(I) oxide surface using facile chemical oxidation processes. High C_{2+} selectivity is then first demonstrated in an H-cell configuration and then successfully transferred into a flow-cell configuration equipped with a gas-diffusion layer (GDL) to increase the current density and improve efficiency, selectivity, and productivity. The flow-cell allows for better control over the operating pH allowing for almost complete CH_4 and H_2 suppression without current limitations, reaching ≈84% FE of C_{2+} products and a half-cell power conversion efficiency (PCE) of ≈50% for C_{2+} products at a partial current density of 336 mA cm^{-2} on the reconstructed Cu surface.

To reconstruct the metallic Cu surface for C_{2+} production, we first grew a CuCl film on an electropolished Cu foil substrate by oxidizing the surface with hydrogen peroxide (H_2O_2) in the presence of a dilute HCl solution (**Figure 1**). The coverage of CuCl on the wet-oxidized Cu surface is tuned by varying the molar ratio of H_2O_2:HCl, allowing the surface morphology of the catalyst to be controlled. A Cu(I) oxide layer is then grown by immersing the CuCl film into a $KHCO_3$ solution (Figure 1). Finally, the reconstructed Cu surface is achieved by electrochemically reducing the formed Cu(I) oxide layer in 0.05 M $KHCO_3$ electrolyte (Figure 1).

To investigate the chemical states and electronic structure of the Cu surface at different steps during the reconstruction process, we performed ex situ soft X-ray absorption spectroscopy (sXAS) studies. We used the Cu L_3-edge as a quantitative means to assess the copper oxidation state as the lower energy transition affords higher spectral resolution and greater contrast between electronic structure changes. The Cu L_3-edge spectra of the reference standards of Cu metal, Cu_2O, and CuO were taken to measure the Cu^0, Cu^+, and Cu^{2+} oxidation states, respectively (**Figure 2**a, and Figure S1, Supporting Information).[27,28] The electropolished copper sample exhibits a Cu L_3-edge similar to that of the Cu metal standard, indicating that the sample is in the Cu^0 oxidation state. After being oxidized with H_2O_2 and hydrolyzed in $KHCO_3$ electrolyte, the copper surface shows a sharper peak near 934 eV consistent with a Cu_2O L_3-edge peak of 933.7 eV.[28] This result suggests that after the wet-oxidation treatment the copper was oxidized to Cu^+. The reduced sample (after linear sweep voltammetry (LSV)) and the sample after 1 h of CO_2-RR shows that the reduced surface is primarily Cu^0. However, a small pre-edge peak exists around 930 eV, which is indicative of a Cu^{2+} oxidation state with an L_3-edge peak position of CuO 930.7 eV.[28]

To provide a quasi-quantitative analysis of the sXAS data, we performed a peak fitting of the measured samples using a linear combination of the Cu, Cu_2O, and CuO reference samples (Figure 2b). The results show that the oxidation state of the initial electropolished Cu state is 100% Cu^0, while the wet-oxidized and hydrolyzed Cu sample is ≈25% composed of the Cu^+ oxidation state. After the surface has been electrochemically reduced via LSV and CO_2-RR, the majority of the sample has been almost entirely reduced to Cu^0. The residual Cu^+ and Cu^{2+} present may be attributed to surface oxides formed upon exposure to air.

X-ray diffraction (XRD) and X-ray photoelectron spectroscopy (XPS) were performed to further confirm the crystalline phase and oxidation state of copper species during the reconstruction process. As shown in Figure 2c, the surface of Cu changed from

Prof. P. Yang
Chemical Sciences Division
Lawrence Berkeley National Laboratory
Berkeley, CA 94720, USA
Prof. P. Yang
Kavli Energy Nanosciences Institute
University of California
Berkeley, Berkeley, CA 94720, USA

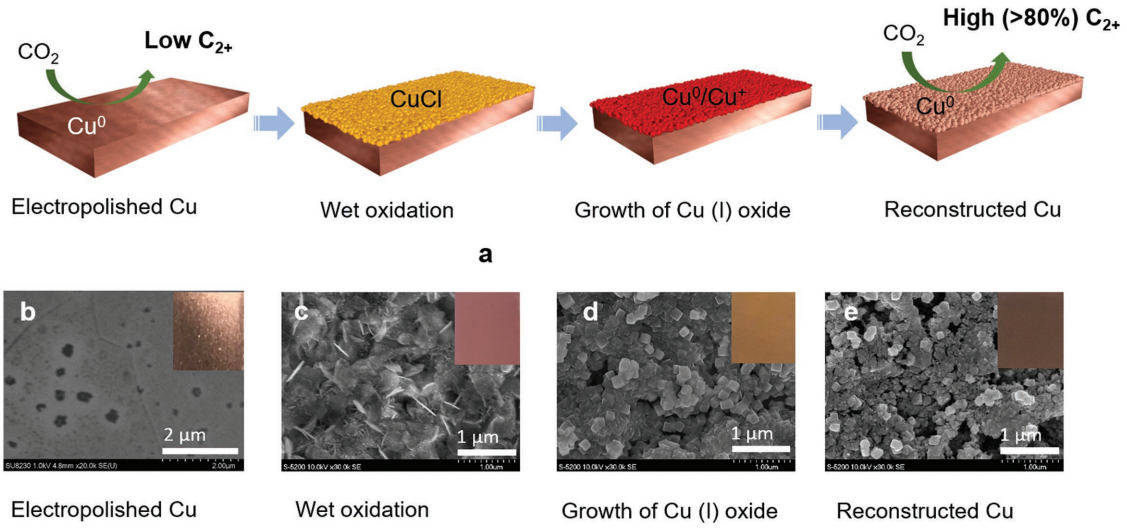

Figure 1. a) Schematic illustration of the surface reconstruction process. b–e) The electropolished Cu surface was wet-oxidized in 60×10^{-3} M [H_2O_2], followed by growth of Cu(I) oxide and finally reconstructed for CO_2-RR.

metallic (Cu^0) to CuCl film as evidenced by the presence of the diffraction peaks at 28.5° and the Cl 2p peak at the binding energy of 199 eV (Figure S2a, Supporting Information) after the wet-oxidation step. After immersion in 0.05 M $KHCO_3$, the CuCl diffraction peak (Figure 2c) and Cl 2p peak (Figure S2a, Supporting Information) are significantly suppressed and the

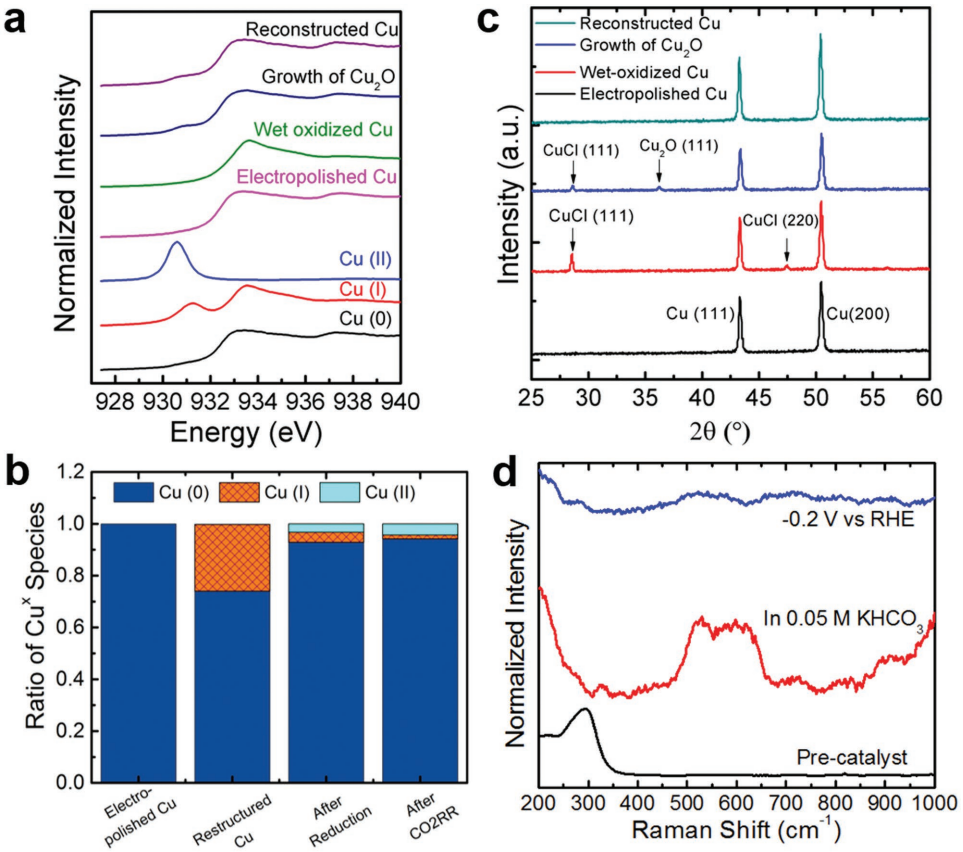

Figure 2. Characterization of surface reconstructed Cu. a) Ex situ Cu L_3-edge soft X-ray absorption spectroscopy (sXAS) spectra of Cu after different process steps and standard Cu (0), Cu (I), and Cu (II) curves. b) Calculated ratio of Cu oxidation states using linear combinations of the Cu (0), Cu (I), and Cu (II) reference standards. c) XRD spectra of electropolished Cu, wet-oxidized Cu, growth of Cu_2O from immersion in $KHCO_3$, and reconstructed Cu. d) Raman spectra of the as-synthesized CuCl-derived precatalyst (black), the Cu catalyst in electrolyte at open-circuit conditions (red), and after the application of reduction potential of −0.2 V versus RHE (blue).

appearance of the diffraction peak at 36.2° (Figure 2c) indicates that the CuCl film is mostly converted to Cu_2O crystals, in good agreement with the observation from scanning electron microscopy (SEM) (Figure 1). After the reduction process (LSV), the XRD of the sample shows diffraction peaks that are characteristic of a pure metallic Cu phase (Figure 2c).

The data from ex situ sXAS and XPS confirm that the reconstructed Cu sample contains primarily a metallic Cu phase with a small amount of oxidized species, which may be the result of exposure to air. We also performed an in situ Raman analysis of the samples during CO_2-RR in 0.1 M $KHCO_3$ electrolyte. As shown in Figure 2d, the peaks in the frequency range of 550–650 cm^{-1}, corresponding to the presence of copper oxide species, appear when immersed in electrolyte and disappear once the sample is subjected to a negative potential of –0.2 V versus RHE. This suggests that Cu^0 is the dominant surface species under CO_2-RR conditions.[29] In summary, all in situ and ex situ characterizations confirm that under reducing conditions the restructured Cu catalyst is composed of metallic copper. However, surface morphology, pore size, and roughness are substantially different for the electropolished and the surface-reconstructed copper samples.

To assess the electrochemical performance of the reconstructed Cu samples, CO_2-RR was performed in 0.05 M $KHCO_3$ in an H-cell configuration. The wet-oxidation process (see the Supporting Information and Figure S3, Supporting Information) of Cu foil was varied by controlling the H_2O_2 concentration in HCl and subsequently performing CO_2-RR to achieve highest C_2H_4:CH_4 ratio, as illustrated in **Figure 3**a. The C_2H_4:CH_4 ratio for the electropolished Cu sample was found to be ≈1, which was subsequently tuned to achieve a tenfold improved ratio under an optimum H_2O_2 concentration of 60×10^{-3} M. Figure 3b shows the Faradaic efficiency (FE) of C_2H_4 and CH_4 versus an applied potential on the surface reconstructed Cu and electropolished Cu surfaces. The C_2H_4 FE on electropolished Cu reached a maximum at 40% in a narrow optimized potential range of –2.0 V versus Ag/AgCl and quickly dropped to less than 25% with a small variation in potential. In the same potential range, a CH_4 FE of >40% was observed, indicating that electropolished Cu is similarly selective for CH_4 generation. In contrast, the surface reconstructed Cu showed an C_2H_4 FE greater than 50% over a wider potential range of –1.9 to –2.4 V versus Ag/AgCl, reaching a maximum of 56% at a potential of –2.0 V versus Ag/AgCl. Interestingly, the CH_4 FE was suppressed down to 5% within the same potential range, resulting in a substantially higher C_2H_4:CH_4 ratio of 11, an order of magnitude higher than the electropolished surface. It is noted that the FE for other products such as CO and H_2 on reconstructed Cu were similar to those observed on electropolished Cu. These results suggest that the surface reconstruction

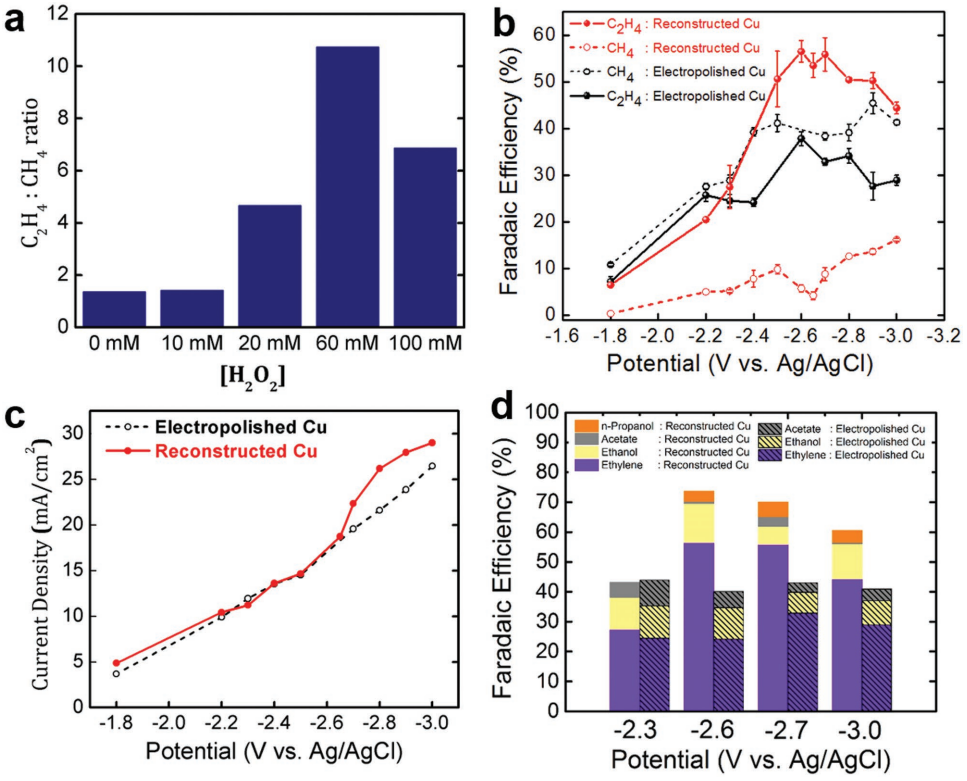

Figure 3. Electrochemical studies in an H-cell configuration. a) C_2H_4:CH_4 product ratios with different concentrations of H_2O_2. b) Faradaic efficiencies (FE) of C_2H_4 and CH_4 for the electropolished and surface reconstructed Cu samples at different applied potentials, demonstrating that surface reconstruction suppresses the CH_4 product pathway and enhances C_2 formation. c) Current density versus applied potential for the electropolished and surface reconstructed Cu samples in a 0.05 M $KHCO_3$ electrolyte. d) FE of C_{2+} products from electropolished and surface reconstructed Cu samples versus applied potential.

process primarily shifts the reaction selectivity from CH_4 to C_2H_4 during the CO_2 reduction reaction, with little effect on other reaction processes.

From a plot of the geometric current density as a function of applied potential (Figure 3c) we can also see that surface reconstruction has no clear effect on the overall activity of Cu toward CO_2-RR in the potential range (–1.8 to –2.0 V vs Ag/AgCl), where the highest FE for C_2H_4 was obtained. This result is different from most reported oxide-derived catalysts which show significant improvements in the total current density compared to polished Cu.[18] It also suggests that the higher C_2H_4 selectivity on surface reconstructed Cu compared to electropolished Cu is not a result from the change in the local pH as frequently observed in other oxide-derived Cu systems. We propose that the surface reconstruction process may change the Cu surface from a stable facet in electropolished Cu such as (111) to a more C_2 selective facet such as (100), leading to a higher selectivity for C_2 products. Figure 3d shows the total FE of C_{2+} products for reconstructed Cu, reaching 73% at a current density of ≈17 mA cm^{-2}, 30% more than that on the electropolished sample. Additionally, in contrast to electropolished Cu which did not yield any *n*-propanol, the surface reconstructed Cu produced nearly 5% *n*-propanol.

The relatively low solubility of CO_2 in aqueous solutions (≈34×10^{-3} M at STP), coupled with the CO_2-carbonate equilibria in an aqueous solution, creates a mass transfer constraint on the CO_2 reduction reaction. Consequently, the primary (steady-state) current density is limited to a maximum value on the order 10 mA cm^{-2} under typical laboratory reaction conditions. An efficient mass transfer of CO_2 to the electrode's surface is therefore key to obtaining industrial scale production of any reduction product. In order to remove the CO_2 mass transfer constraint noted above, and to achieve higher productivity (i.e., current density), we utilized a gas diffusion electrode (GDE) to greatly reduce the diffusion pathway of CO_2 to the catalyst's surface. Furthermore, the GDE environment allowed us to perform the reaction in an alkaline environment which favors C_{2+} selectivity.[30–32] In this system, the catalyst is deposited onto the GDE, while CO_2 reduction proceeds on the catalyst surface in the electrolyte near the gaseous CO_2 and liquid interface.

To create the catalyst layer on a GDL, we performed the wet-oxidation process described previously on a thermally evaporated ≈300 nm Cu layer on a GDL (Figure S4, Supporting Information). We again optimized the wet-oxidation process to achieve high C_{2+} product selectivity on the GDE. To measure the CO_2-RR selectivity of the surface reconstructed Cu surface on a GDL, the H-cell configuration was replaced by a flow-cell configuration. The resulting electrochemical performance using 1 M $KHCO_3$ as an electrolyte is shown in **Figure 4**a for both the surface reconstructed and evaporated Cu catalysts. As can be seen, both the partial current density and selectivity

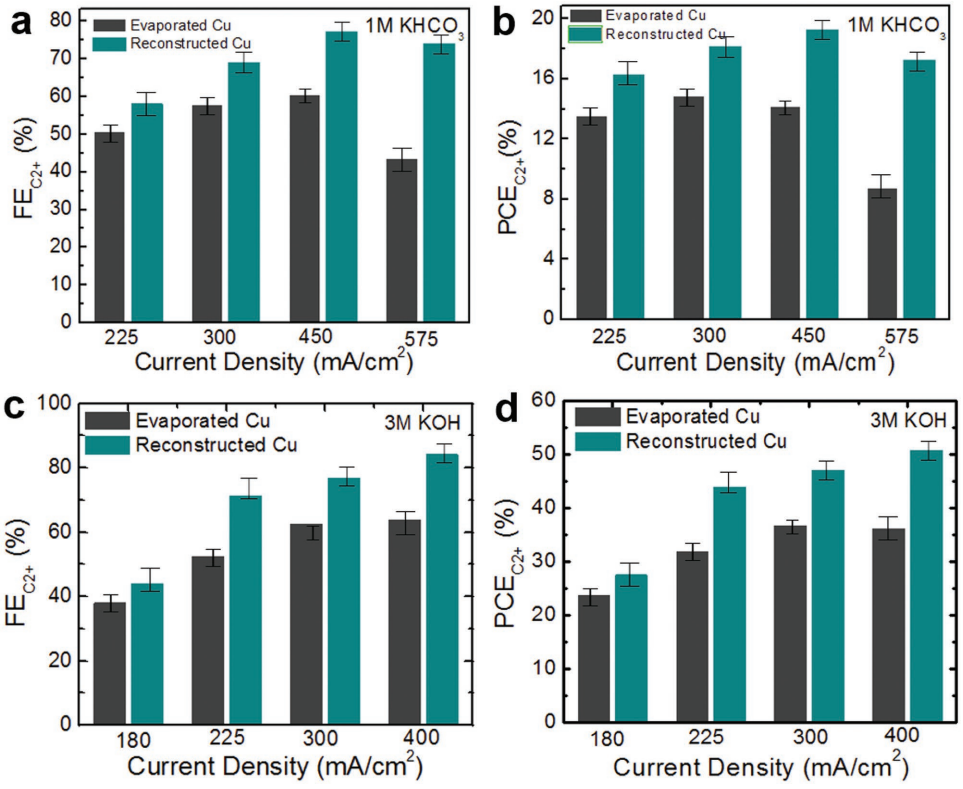

Figure 4. Electrocatalytic CO_2 reduction activity in the flow-cell configuration. a) FE of C_{2+} products in 1 M $KHCO_3$ for the evaporated and surface reconstructed Cu samples with different applied current densities. b) Power conversion efficiency (PCE) comparison for the evaporated Cu and surface reconstructed Cu samples as a function of current density in 1 M $KHCO_3$. c) FE of C_{2+} products in 3 M KOH for the evaporated and reconstructed Cu samples with different applied current densities. d) PCE comparison for the evaporated Cu and surface reconstructed Cu samples as a function of current density in 3 M KOH.

toward C_{2+} products improved in the flow-cell configuration, with a C_{2+} selectivity of 77% achieved at 450 mA cm^{-2} and an applied potential of −1.8 V versus RHE. Most importantly, CH_4 selectivity was drastically suppressed to below 1% in the flow-cell configuration in contrast to ≈10% selectivity in H-cell configuration. At these high current densities the local pH can be significantly increased, leading to a suppression of methane production and an increase in C_{2+} selectivity as described elsewhere.[33] The half-cell PCE (see the Experimental Section for definition and calculation) for C_{2+} products is then compared for the as-evaporated and surface reconstructed Cu, as shown in Figure 4b to evaluate the performance of the cathode alone. At all applied current densities, the PCE is found to be improved by 5–10% in case of surface reconstructed Cu, with the maximum PCE of 18% at 450 mA cm^{-2}. It is also worth noting that the expected increase in the local pH at high current densities has not been accounted for in the measured applied potential.

It has been reported that the reaction overpotential for CO_2-RR can be reduced and therefore selectivity for C_{2+} products and subsequently the PCE can be significantly improved by performing the reaction in highly alkaline conditions.[30–32] Therefore, the CO_2 reduction performance of the reconstructed Cu sample was tested under highly alkaline (3 M KOH) conditions, again in the flow-cell configuration. Figure 4c shows the FE of C_{2+} products (ethylene, ethanol, propanol, and acetate) of reconstructed Cu and the as-evaporated Cu at various current densities. At all the measured current densities, the C_{2+} selectivity is found to be improved by 15–25% after surface reconstruction. At the optimum overall current density of 400 mA cm^{-2} and applied voltage of −0.68 V versus RHE, the highest FE of 84% was measured for C_{2+} products on the reconstructed Cu sample. The record high (Table S1, Supporting Information) partial current density for C_{2+} products was measured to be 336 mA cm^{-2}. The distribution of all the products from CO_2-RR on reconstructed Cu at different current densities is shown in Figure S5 (Supporting Information). At lower current densities, the catalyst is more prone to produce C_1 (i.e., CO) products. With an increase in current, C_1 production is reduced and C_{2+} products are increased drastically with a peak occurring at 400 mA cm^{-2}. With further increases in current density, the hydrogen evolution reaction eventually increases, lowering the Faradaic efficiency for C_{2+} products. The half-cell PCE of the as-evaporated and surface reconstructed Cu samples, shown in Figure 4d, reveals that the PEC is significantly improved by using 3 M KOH as an electrolyte, with the highest PCE measured of 50% at overall current of 400 mA cm^{-2}.

In conclusion, we have developed a surface reconstruction process to tune the CO_2-reduction selectivity of a Cu surface. Using a facile wet-oxidation process, the Cu catalyst can be tuned from one that is CH_4 selective to one that favors C_{2+} products. Importantly, the surface reconstruction process was extended to a gas-diffusion electrode, allowing for the demonstration of commercially interesting current densities while maintaining high selectivities toward C_{2+} products. We demonstrated a record C_{2+} selectivity of 84% at a partial current density of 336 mA cm^{-2} and at a half-cell power conversion of up to 50% on the surface reconstructed Cu catalyst. We propose that the surface reconstruction process can also be applied to Cu catalysts with different morphologies to further enhance both selectivity and current density for the production of multicarbon products from both CO_2 and CO reduction.

Supporting Information

Supporting Information is available from the Wiley Online Library or from the author.

Acknowledgements

M.G.K., C.-T.D., and A.S. contributed equally to this work. This work was financially supported by the Ontario Research Fund: Research Excellence Program, the Natural Sciences and Engineering Research Council (NSERC) of Canada, the CIFAR Bio-Inspired Solar Energy program. The authors thank D. Kopilovic and R. Wolowiec for electrochemical cell design and setup. The authors acknowledge Toronto Nanofabrication Centre (TNFC) and Ontario Centre for the Characterization of Advanced Materials (OCCAM) for sample preparation and characterization facilities. The authors acknowledge Dr. Taotao Zhuang for his help with Figure 1. X-ray spectroscopy described in this paper was performed at the Canadian Light Source, which is supported by the Canada Foundation for Innovation, Natural Sciences and Engineering Research Council of Canada, the University of Saskatchewan, the Government of Saskatchewan, Western Economic Diversification Canada, the National Research Council Canada, and the Canadian Institutes of Health Research. The authors thank T. Regier for XAS support. A.S. wishes to thank Fonds de Recherche du Quebec – Nature et Technologies (FRQNT) for support in the form of postdoctoral fellowship award. M.K. acknowledges Banting postdoctoral fellowship from Government of Canada. T.B. thanks Hatch for a Graduate Scholarship for Sustainable Energy Research. P.D.L. and O.S.B. thank NSERC for financial support in the form of the Canada Graduate Scholarship – Doctoral (CGS-D) award and NSERC Post-Doctoral Fellowship, respectively. M.B.R. is grateful for support from the CIFAR Bio-Inspired Solar Energy program.

Conflict of Interest

The authors declare no conflict of interest.

Keywords

CO_2 electroreduction, Cu-based catalysts, flow-cells, hydrocarbons

Received: July 29, 2018
Revised: September 9, 2018
Published online:

[1] J. Qiao, Y. Liu, F. Hong, J. Zhang, *Chem. Soc. Rev.* **2014**, *43*, 631.
[2] J.-P. Jones, G. K. S. Prakash, G. A. Olah, *Isr. J. Chem.* **2014**, *54*, 1451.
[3] C. Graves, S. D. Ebbesen, M. Mogensen, K. S. Lackner, *Renewable Sustainable Energy Rev.* **2011**, *15*, 1.
[4] M. Jouny, W. Luc, F. Jiao, *Ind. Eng. Chem. Res.* **2018**, *57*, 2165.
[5] G. O. Larrazábal, A. J. Martín, J. Pérez-Ramírez, *J. Phys. Chem. Lett.* **2017**, *8*, 3933.
[6] O. S. Bushuyev, P. De Luna, C. T. Dinh, L. Tao, G. Saur, J. van de Lagemaat, S. O. Kelley, E. H. Sargent, *Joule* **2018**, *2*, 825.

[7] K. P. Kuhl, E. R. Cave, D. N. Abram, T. F. Jaramillo, *Energy Environ. Sci.* **2012**, *5*, 7050.
[8] D. Raciti, C. Wang, *ACS Energy Lett.* **2018**, *3*, 1545.
[9] H. Mistry, A. S. Varela, C. S. Bonifacio, I. Zegkinoglou, I. Sinev, Y.-W. Choi, K. Kisslinger, E. A. Stach, J. C. Yang, P. Strasser, *Nat. Commun.* **2016**, *7*, 12123.
[10] D. Ren, B. S.-H. Ang, B. S. Yeo, *ACS Catal.* **2016**, *6*, 8239.
[11] D. Ren, N. T. Wong, A. D. Handoko, Y. Huang, B. S. Yeo, *J. Phys. Chem. Lett.* **2016**, *7*, 20.
[12] T.-T. Zhuang, Z.-Q. Liang, A. Seifitokaldani, Y. Li, P. De Luna, T. Burdyny, F. Che, F. Meng, Y. Min, R. Quintero-Bermudez, C. T. Dinh, Y. Pang, M. Zhong, B. Zhang, J. Li, P.-N. Chen, X.-L. Zheng, H. Liang, W.-N. Ge, B.-J. Ye, D. Sinton, S.-H. Yu, E. H. Sargent, *Nat. Catal.* **2018**, *1*, 421.
[13] A. A. Peterson, F. Abild-Pedersen, F. Studt, J. Rossmeisl, J. K. Norskov, *Energy Environ. Sci.* **2010**, *3*, 1311.
[14] A. A. Peterson, J. K. Nørskov, *J. Phys. Chem. Lett.* **2012**, *3*, 251.
[15] A. Eilert, F. Cavalca, F. S. Roberts, J. Osterwalder, C. Liu, M. Favaro, E. J. Crumlin, H. Ogasawara, D. Friebel, L. G. M. Pettersson, A. Nilsson, *J. Phys. Chem. Lett.* **2017**, *8*, 285.
[16] X. Feng, K. Jiang, S. Fan, M. W. Kanan, *J. Am. Chem. Soc.* **2015**, *137*, 4606.
[17] P. De Luna, R. Quintero-Bermudez, C.-T. Dinh, M. B. Ross, O. S. Bushuyev, P. Todorović, T. Regier, S. O. Kelley, P. Yang, E. H. Sargent, *Nat. Catal.* **2018**, *1*, 103.
[18] H. Mistry, A. S. Varela, C. S. Bonifacio, I. Zegkinoglou, I. Sinev, Y.-W. Choi, K. Kisslinger, E. A. Stach, J. C. Yang, P. Strasser, B. R. Cuenya, *Nat. Commun.* **2016**, *7*, 12123.
[19] M. Favaro, H. Xiao, T. Cheng, W. A. Goddard, J. Yano, E. J. Crumlin, *Proc. Natl. Acad. Sci. USA* **2017**, *114*, 6706.
[20] A. Dutta, M. Rahaman, N. C. Luedi, M. Mohos, P. Broekmann, *ACS Catal.* **2016**, *6*, 3804.
[21] W. Tang, A. A. Peterson, A. S. Varela, Z. P. Jovanov, L. Bech, W. J. Durand, S. Dahl, J. K. Norskov, I. Chorkendorff, *Phys. Chem. Chem. Phys.* **2012**, *14*, 76.
[22] Y. Pang, T. Burdyny, C.-T. Dinh, M. G. Kibria, J. Z. Fan, M. Liu, E. H. Sargent, D. Sinton, *Green Chem.* **2017**, *19*, 4023.
[23] T. Burdyny, P. J. Graham, Y. Pang, C.-T. Dinh, M. Liu, E. H. Sargent, D. Sinton, *ACS Sustainable Chem. Eng.* **2017**, *5*, 4031.
[24] T. T. H. Hoang, S. Ma, J. I. Gold, P. J. A. Kenis, A. A. Gewirth, *ACS Catal.* **2017**, *7*, 3313.
[25] K. Jiang, R. B. Sandberg, A. J. Akey, X. Liu, D. C. Bell, J. K. Nørskov, K. Chan, H. Wang, *Nat. Catal.* **2018**, *1*, 111.
[26] C. W. Li, J. Ciston, M. W. Kanan, *Nature* **2014**, *508*, 504.
[27] P. Jiang, D. Prendergast, F. Borondics, S. Porsgaard, L. Giovanetti, E. Pach, J. Newberg, H. Bluhm, F. Besenbacher, M. Salmeron, *J. Chem. Phys.* **2013**, *138*, 024704.
[28] M. Grioni, J. B. Goedkoop, R. Schoorl, F. M. F. de Groot, J. C. Fuggle, F. Schäfers, E. E. Koch, G. Rossi, J. M. Esteva, R. C. Karnatak, *Phys. Rev. B* **1989**, *39*, 1541.
[29] L. Mandal, K. R. Yang, M. R. Motapothula, D. Ren, P. Lobaccaro, A. Patra, M. Sherburne, V. S. Batista, B. S. Yeo, J. W. Ager, J. Martin, T. Venkatesan, *ACS Appl. Mater. Interfaces* **2018**, *10*, 8574.
[30] S. Ma, M. Sadakiyo, R. Luo, M. Heima, M. Yamauchi, P. J. A. Kenis, *J. Power Sources* **2016**, *301*, 219.
[31] S. Verma, X. Lu, S. Ma, R. I. Masel, P. J. A. Kenis, *Phys. Chem. Chem. Phys.* **2016**, *18*, 7075.
[32] C.-T. Dinh, T. Burdyny, M. G. Kibria, A. Seifitokaldani, C. M. Gabardo, F. P. García de Arquer, A. Kiani, J. P. Edwards, P. De Luna, O. S. Bushuyev, C. Zou, R. Quintero-Bermudez, Y. Pang, D. Sinton, E. H. Sargent, *Science* **2018**, *360*, 783.
[33] R. Kas, R. Kortlever, A. Milbrat, M. T. M. Koper, G. Mul, J. Baltrusaitis, *Phys. Chem. Chem. Phys.* **2014**, *16*, 12194.